Similarities and differences between gliding glow and gliding arc discharges

St Kolev[1,2], A Bogaerts[1]

[1]Research group PLASMANT, Department of Chemistry, University of Antwerp, Universiteitsplein 1, B-2610 Antwerp, Belgium

[2]Faculty of Physics, Sofia University, 5 James Bourchier Boulevard, 1164 Sofia, Bulgaria

E-mail: skolev@phys.uni-sofia.bg

E-mail: annemie.bogaerts@uantwerpen.be

Abstract. In this work we have analyzed the properties of a gliding DC discharge in argon at atmospheric pressure. Despite the usual designation of these discharges as "gliding arc discharges", it was found previously that they operate in two different regimes – glow and arc. Here we analyze the differences in both regimes by means of two dimensional fluid modeling. In order to address different aspects of the discharge operation, we use two models – Cartesian and axisymmetric in a cylindrical coordinate system. The obtained results show that the two types of discharges produce a similar plasma column for a similar discharge current. However, the different mechanisms of plasma channel attachment to the cathode could produce certain differences in the plasma parameters (i.e., arc elongation), and this can affect gas treatments applications.

PACS numbers: 52.50.Dg, 52.50.Nr, 52.65.Kj, 52.80.Mg

Keywords: gliding arc discharge, sliding arc discharge, fluid plasma model, atmospheric pressure plasmas, argon plasma

1. Introduction

Gliding arc discharges (GADs) are DC or low frequency AC discharges produced usually between two diverging electrodes. The plasma channel moves along the electrodes due to a forced gas flow and when its length becomes very long, the discharge diminishes and it reignites at the shortest electrode distance. GADs attracted considerable interest [1] because of their ability to produce a non-equilibrium plasma at atmospheric pressure. At the same time, a considerable power can be applied while keeping the gas temperature relatively low and avoiding the appearance of a classical thermal arc discharge. They also provide a good selectivity and efficiency in many different plasma chemistry applications for gas reforming and treatment [1–3]. The simple design, the affordable set-up and the operation under atmospheric pressure make them even more attractive from industrial point of view.

Despite the simplicity of building GADs, they are rather difficult for experimental diagnostics and theoretical studies. This is mainly due to the non-stationary nature of the discharge and often, due to the lack of good repeatability between the discharge cycles. Moreover, fast photographs of the discharge [4] show the existence of two different regimes of operation – arc and glow. In the case of an arc discharge, the discharge is sustained by thermo-field electron emission from the cathode and it is accompanied with the formation of a tiny cathode spot. In the case of a glow discharge, the discharge is sustained by secondary electron emission due to ion bombardment. Experimental studies [4] even show that both regimes could be present in a single cycle of the plasma channel evolution.

In this work we present a theoretical study of both gliding arc and gliding glow discharges based on two dimensional fluid plasma models. The work aims at describing the mechanisms governing the gliding of the plasma channel and at pointing out the similarities and the differences between both regimes and the effect of the discharge regime on the overall discharge performance.

The paper has the following structure: In section 2 we briefly describe the model developed for the GAD description. The obtained results are presented in section 3. In subsection 3.1 we discuss the discharge properties based on a 2D axisymmetric model, while in subsection 3.2 we discuss the discharge gliding mechanisms based on results from a 2D model in a Cartesian coordinate system.

2. Model description

In this work we use two different models in argon – a 2D model in a Cartesian coordinate system and a 2D model in a cylindrical coordinate system assuming axial symmetry. Because of the limited dimensionality of the models, neither of them can exactly describe the considered discharge. However, they are sufficient to describe the qualitative behavior of the discharge and to provide valuable results. This approach was exploited in our previous work [5] and it was found to be a good compromise between quality of the obtained results and the computational time needed for the calculations.

A detailed description of the models can be found in an accompanying file, provided online as supporting information to this paper. A brief description of the major model equations used here is given in Appendix A.

2.1. 2D axisymmetric model

The axisymmetric plasma model used here is based on the axisymmetric model described in [5] with two differences: a) the cathode heating is neglected and therefore we do not solve equations (12) and (13) in [5]; b) we include additional loss terms in all balance equations (i.e. all except in the Poisson equation). Neglect the cathode heating is indeed justified because it was found in [5] that it has a minor influence. The aim of the additional loss terms is to effectively account for the stretching of the gliding discharge

as a result of the gas flow and thus to account for the convective processes. This was not accounted for in our previous model, but it is included here since it allows our 2D model to better represent the specific properties of GADs related to the convection process, which is in fact a 3D problem.

We consider the effect of the gas convection as a simple stretching of the arc which redistributes the species and their energy over a larger volume. This means that if we consider a plasma channel and if we stop the heating and particle production processes, the species densities and energies will gradually decrease in time as a result of the introduced effective convective losses. In practice, in the axisymmetric model from [5] we introduce the loss terms on the right hand side of equations 1, 6 and 10 according to the numbering in [5] or equations A-1, A-2 and A-6, as presented in Appendix A. These terms are introduced as effective loss processes with a constant frequency ν_{elong}, equal for all equations. Thus the loss terms will be proportional to $-\alpha\nu_{\text{elong}}$, where α represents the conserved variable i.e. $\alpha = n_{\text{e}}$, n_{Ar^+}, $n_{\text{Ar}_2^+}$, $n_{\text{Ar(4s)}}$, $n_{\text{Ar(4p)}}$, $n_{\text{Ar}_2^*}$, $n_{\text{e}}\overline{\varepsilon}_{\text{e}}$, $\rho_{\text{g}}C_pT_{\text{g}}$. Here the first 6 variables are the densities of the considered species: e – electrons, Ar^+ – argon ions, Ar_2^+ – argon molecular ions, Ar (4s) – all 4s levels considered as a single lumped excitation level, Ar (4p) – all 4p levels considered as a single lumped excitation level, and Ar_2^* – which includes $\text{Ar}_2(^1\Sigma_u^+)$ and $\text{Ar}_2(^3\Sigma_u^+)$ excited molecules. $\overline{\varepsilon}_{\text{e}}$ is the averaged electron energy, ρ_{g} is the gas density, C_p is the gas heat capacity and T_{g} is the gas temperature. ν_{elong} has a unit of frequency [1/s] but it is related to the elongation speed of the plasma channel. Below we give more details about the definition of ν_{elong} and its relation to the real convection process.

Let us consider an elementary domain with volume Ω and length l in the direction of elongation. As a result of the elongation with speed v_{elong} for time $\text{d}t$, the plasma channel length will increase with $\text{d}l = v_{\text{elong}}\text{d}t$ and the domain volume will increase with $\text{d}\Omega = \text{d}lS_{\text{tr}}$, where S_{tr} is the transverse cross section of the plasma channel. If we take into account that for some variables there is a minimum (background) value (α_{bg}) different from zero (like for example the gas temperature $T_{\text{g}} = 293$ K) we can express the variation (reduction) of the conserved variable α as the difference between the initial (α) and the value after elongation α_{elong}:

$$\text{d}\alpha = \alpha_{\text{elong}} - \alpha = \frac{\alpha\Omega + \alpha_{\text{bg}}\text{d}\Omega}{\Omega + \text{d}\Omega} - \alpha = -\frac{(\alpha - \alpha_{\text{bg}})\text{d}\Omega}{\Omega + \text{d}\Omega} \approx$$
$$-\frac{(\alpha - \alpha_{\text{bg}})\text{d}\Omega}{\Omega} = -(\alpha - \alpha_{\text{bg}})\frac{\text{d}l}{l} = -(\alpha - \alpha_{\text{bg}})v_{\text{elong}}\frac{\text{d}t}{l} \tag{1}$$

where we have used that the variables are conserved i.e. $\alpha\Omega + \alpha_{\text{bg}}\text{d}\Omega = \alpha_{\text{elong}}(\Omega + \text{d}\Omega)$ and the fact that $\text{d}\Omega \ll \Omega$. Thus for the effective loss term due to convection we obtain:

$$\frac{\text{d}\alpha}{\text{d}t} = -(\alpha - \alpha_{\text{bg}})v_{\text{elong}}/l = -(\alpha - \alpha_{\text{bg}})\nu_{\text{elong}} \tag{2}$$

In our simulations ν_{elong} is constant (a parameter) in every model run. Since the length of the plasma channel increases in time, this means that the elongation speed will increases in time too. Note that ν_{elong} is taken as a constant not only in time but also in space and it is the same in the whole domain. In reality probably this is not exactly true

since the gas velocity is different in the different regions – close to the walls and at the discharge axis.

The above approach allows us approximately to take into account the convection processes in the gliding discharge while representing the plasma channel by using a 2D axisymmetric model. In the model, we take α_{bg} to be zero for all variables except for the gas temperature: $T_{\mathrm{g,bg}} = 293$ K. Note that this approach allows also the derivation of a steady state solution which corresponds to an infinite expansion of the discharge. Although in this work we will present results for the axially symmetric geometry for a time of 200 μs, the steady state solution obtained in this way is rather close to the solution at 200 μs and usually the difference is less than 30%.

The geometry considered in this model is presented in figure 1(a). It is a simple rectangle with 6 mm distance between the electrodes.

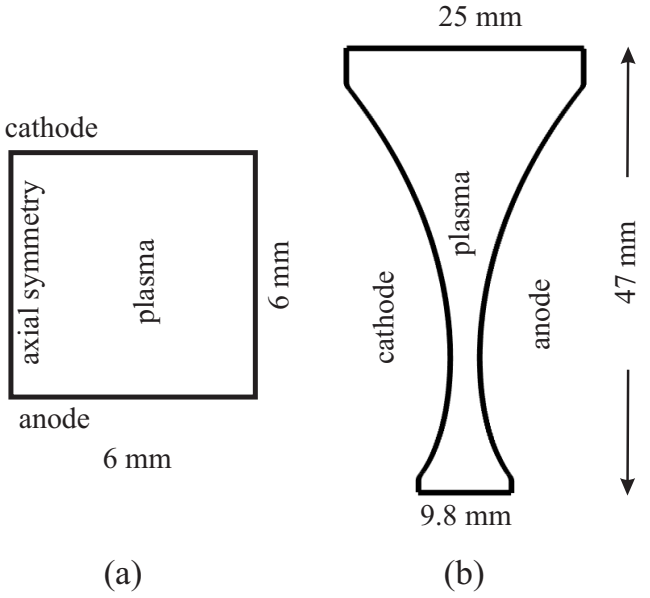

Figure 1. Geometries considered in the models: (a) 2D axisymmetric and (b) 2D Cartesian model geometries.

The argon chemistry used is the same as in [5]. Note that in [5] there is a typing error in table 2 process 26: the rate coefficient is 2.5×10^{-44} m^6/s and not 3.3×10^{-44} m^6/s as it is written.

2.2. 2D Cartesian model

The Cartesian model is the same as the Cartesian model presented in [5]. It considers the same argon chemistry, equations and boundary conditions. The only difference is the slightly reduced geometry – we use the same electrode shape again with minimum distance between them of 3.2 mm but the domain is reduced in the z direction since in this work we will not consider a whole cycle of the discharge gliding. The geometry modification allows the reduction of the computational time.

In both models, the external circuit is represented by a fixed voltage source $V_{\text{source}} = 3700$ V and serially connected resistor R_{b}.

Note that in the models, due to the relatively low current values considered here, we have neglected the effect of the electrode sputtering and evaporation on the discharge operation. In [5] we have shown that the electrode remains relatively cold.

3. Results and discussions

The discussion and presentation of the obtained results will start with the axisymmetric model since it allows to better demonstrate some of the properties of the two discharges. The conditions of the simulations are again similar to the reference experiment [6, 7], i.e., an atmospheric pressure argon discharge with current of about 31 mA and gas flow of 10 L/min.

3.1. Quasi-gliding cylindrical DC discharge in 2D axisymmetric geometry

All presented results here are at time $t = 200\ \mu s$ which corresponds approximately to the initial stages of discharge gliding, i.e. to the second frame in the photographs included in figure 2 of [6]. The value of ν_{elong} is a parameter which will be varied in the different simulations but in order to have more realistic conditions we estimate it roughly from the fast photographs presented in [6]. Immediately after the gas breakdown at the shortest electrode distance, the elongation velocity is estimated to be around $v_{\text{elong}} = 35$ m/s for a length of approximately 7 mm and thus we take $\nu_{\text{elong}} = 5$ kHz as a reference value.

In figure 2 we present results for the electron density n_{e} for both regimes. The simulation parameters are noted in the figure caption. The glow and arc regimes are obtained by switching off the field and secondary electron emission respectively. This is done by modification of the two parameters FEF and γ_s as noted in the figure caption. The ballast resistor is slightly different in both cases in order to provide the same discharge current $I_{\text{ga}} = 31$ mA, which is similar to the typical experimental value [6].

Visually both discharges differ mainly in the cathode region and they are very similar in the rest of the domain. The difference in the cathode region is expected because of the different electron emission process, which modifies the cathode fall region. In the case of an arc with field emission (figure 2(a)) the current near the cathode is concentrated in a tiny channel and a small cathode spot is formed in order to provide the strong electric field needed for efficient field emission. In the case of a glow discharge (figure 2(b)), the cathode spot is much wider in order to provide a large enough surface for the ion-induced secondary electron emission.

The similarities and the differences could be better seen with 1D plots of the plasma parameters. The electric potential along the symmetry axis (r=0) is plotted in figure 3. The small plots inside the figure are a zoom on the electrode regions. The profiles are practically identical in the anode region and the bulk plasma, and they differ in the cathode region only. The cathode fall in the arc is in the order of 15 V while for the

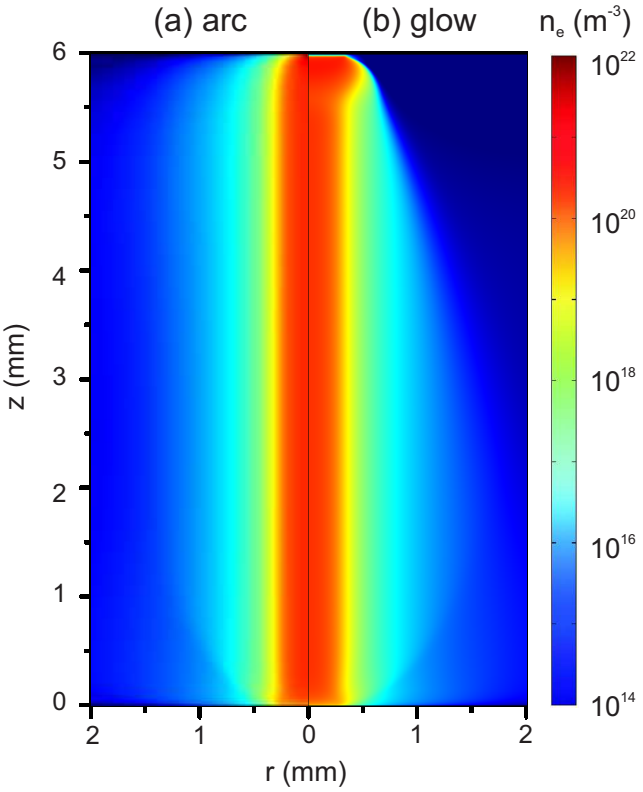

Figure 2. Electron density distribution, calculated with the axisymmetric model in the case of an arc (a) and a glow (b) discharge at $t = 0.2$ ms. The following simulation parameters are used: a) $I_{\mathrm{ga}} = 31$ mA, FEF $= 200$, $\gamma_s = 0$, $R_{\mathrm{b}} = 115.5$ kΩ, $\nu_{\mathrm{elong}} = 5$ kHz; b) $I_{\mathrm{ga}} = 31$ mA, FEF $= 0$, $\gamma_s = 0.02$, $R_{\mathrm{b}} = 110$ kΩ, $\nu_{\mathrm{elong}} = 5$ kHz. The anode is found at $z = 0$, whereas the cathode is positioned at $z = 6$ mm.

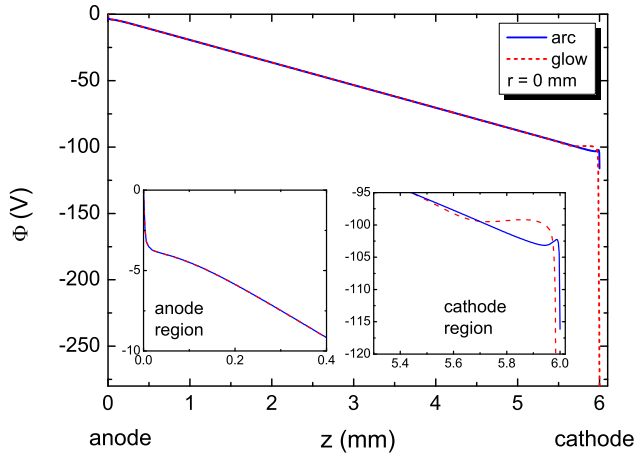

Figure 3. Electric potential profiles along the symmetry axis ($r = 0$). The simulation conditions are the same as in figure 2.

glow discharge it is around 190 V.

The electron density profiles along the symmetry axis (figure 4) show differences again only in the cathode region. A similar behavior is observed also for the other

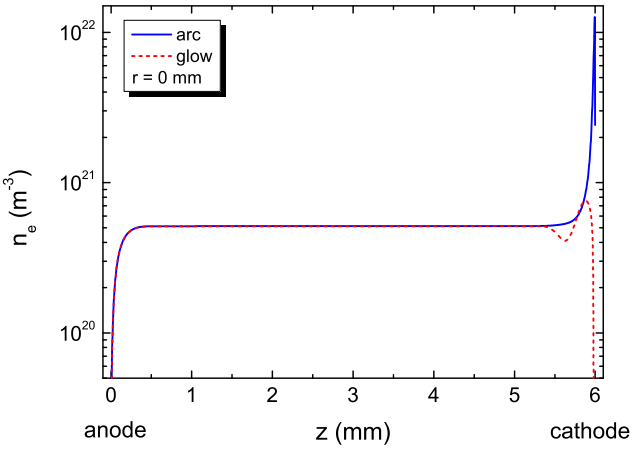

Figure 4. Electron density along the symmetry axis ($r = 0$). The simulation conditions are the same as in figure 2.

plasma parameters like the gas temperature and the densities of the other species.

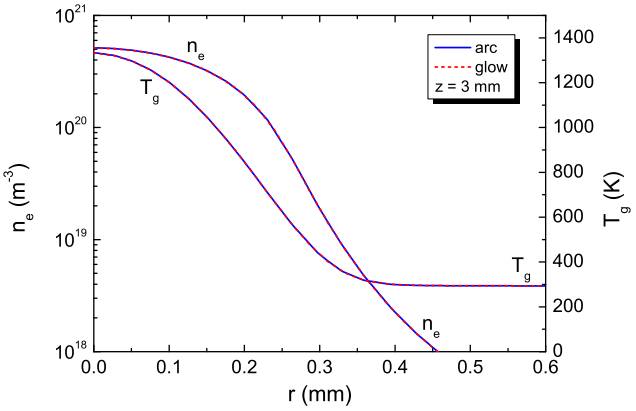

Figure 5. Radial distribution of the electron density and gas temperature at $z = 3$ mm (i.e., in the middle between cathode and anode). The simulation conditions are the same as in figure 2.

In figure 5 the radial variation of n_e and T_g at $z = 3$ mm (i.e., in the middle between cathode and anode) shows practically overlapping results for both regimes.

Overall, the results show that only a small region around the cathode is really different in the case of glow and arc discharges. For the conditions considered here, the typical size of this region is around 0.5 mm. If we compare this size with the plasma channel length, which is at least several millimeters even at the shortest interelectrode distance, we can conclude that there is no considerable difference in the produced plasma in both cases. The plasma channel, outside the near-electrode regions, does not depend on the cathode emission process and it is practically the same. Note also that the plasma channel shows relatively local behavior – if the discharge current is the same, the central regions of the plasma channel remain the same, regardless of the discharge length. This conclusion is especially important when we consider the gliding discharge

in the framework of gas treatment. We could expect that if both discharges have similar length and shape, they will have similar impact on the treated gas.

If we return back to figure 3 we can notice that the two discharges have rather different applied voltage, producing a similar plasma conducting the same current. For the glow regime, the discharge voltage is $V_\mathrm{d} = 299$ V, while for the arc it is only $V_\mathrm{d} = 122$ V. This means also a very different total power: 9.17 W and 3.78 W, respectively. Apparently, the higher power value for the glow discharge is related to the much higher cathode fall (around 190 V). Therefore, practically the same amount of plasma is produced by very different power values. This difference is of practical importance when using the gliding discharge in applications where the power efficiency is a key issue, like for example CO_2 decomposition on an industrial scale.

Note that a similar behavior was also observed in experiments. In [4] both gliding arc and glow discharges in air have been studied. The voltage waveforms in [4] show that 1 ms after the breakdown the glow discharge voltage is around 400 V (figure 3 in [4]) while it is nearly 200 V in the case of an arc discharge (figure 8 in [4]). Thus, this behavior is not specific for our model conditions (argon discharge with 31 mA current) but it is a more general trend stemming from the electron emission process at the cathode.

In [4] the different regimes were achieved by modifying the surface properties of the electrodes. In order to observe a glow discharge, the electrodes were well conditioned, while they were unconditioned for the arc discharge. This is in agreement with our modeling approach. A well-conditioned electrode, i.e., polished and cleaned, corresponds to a field enhancement factor close to 1 (FEF ~ 1) and thus the electric field is not strong enough to drive the field emission and the discharge is sustained by secondary electron emission (SEE) – thus a glow discharge. If the electrodes are not pre-treated, then usually FEF > 100 because of surface protrusions and impurities [8] causing a local amplification of the electric field which could be sufficient for field emission. Note that in terms of efficiency, the field emission (FE) is much more effective than the secondary electron emission – in FE, several electrons are emitted per single ion while for SEE, only one electron is emitted for many ions reaching the cathode.

The results in [4] also comply with the mechanism of the arc gliding we have described in [5] and which are also observed in other experiments [6, 9, 10]. In [5] we stressed that in the case of an arc discharge, the presence of emitting centers (protrusions or impurities) modifies the arc gliding to a jumping motion of the cathode spot, as also observed in figure 8 in [4].

We have also compared the obtained discharge voltages with the experimental data available in [6] and additional data obtained by private communication with the authors of [6]. The data inspection shows discharge voltage values relatively close to the obtained one - in the order of 80-160 V in the experiments versus 122 V in the model. Note however that the comparison is not completely reliable because of technical difficulties in finding the exact correspondence between the voltage/current signal and the fast photographs in [6, 7].

In order to further generalize our study, we have modeled the two discharge regimes without gas heating, i.e. keeping the gas at room temperature. This extends our conclusions to gases which are not so much prone to contraction as is the case for an argon discharge. The results show the same behavior – the plasma parameters differ only near the cathode surface.

3.2. Comparison between arc and glow gliding discharge within a 2D Cartesian geometry.

The above results show that if the plasma channels in both regimes have identical shapes and if they are subject to the same convective effects, we observe very similar properties outside the cathode regions. Are there any circumstances under which the above assumptions are violated for the two different regimes of operation? Our study shows that the answer is yes and for certain conditions the different mechanisms of attachment of the plasma channel at the cathode may introduce differences in the plasma channel length and stretching rate. In [5] we have commented that in the arc regime, the cathode spot is firmly attached to the emission center. The attachment point is expected to be a surface protrusion or some kind of contamination, causing a local increase of the electric field and thus providing proper conditions for field electron emission. Without such a field amplification center, our axisymmetric model shows that the discharge tends to operate in a glow regime. However, the different mechanisms of the plasma column attachment to the cathode may change the convective elongation of the plasma column. For example in the case of a glow regime, the 2D Cartesian model shows that the cathode contact point (root) tends to follow the anode contact point (figure 6). This motion is self-consistently calculated within the model and it is determined by the bending of the plasma channel and the resulting increase of the electric field between the cathode and the plasma channel downstream. A similar behavior is observed also in the experiments in air [4].

On the other hand, in the case of an arc operation (figure 7), the plasma channel is firmly attached to the electron emission position and it could remain attached for a long time. The cathode root of the arc moves downstream by new breakdowns [5]. This jumping motion of the arc cathode root is accompanied with jumps (drops) in the discharge voltage due to the fast reduction of the plasma channel length. In [5] we have modeled this kind of movement by artificially initiating new breakdowns between the cathode and the plasma channel, following the movement of the anode root. In this case the resulting displacement of the arc is similar to the glow discharge. However, we should stress that depending on the conditions of the surface (presence of emission centers), the appearance of a new breakdown could be hindered by the lack of such centers and the discharge may remain attached to the same point at the cathode for a long time (figure 7, $t = 0.35$ ms). This causes a more intensive stretching of the arc on the left hand side (the side of the cathode) and it could modify slightly the plasma column there. Moreover, the longer length of the discharge might have a different effect in the

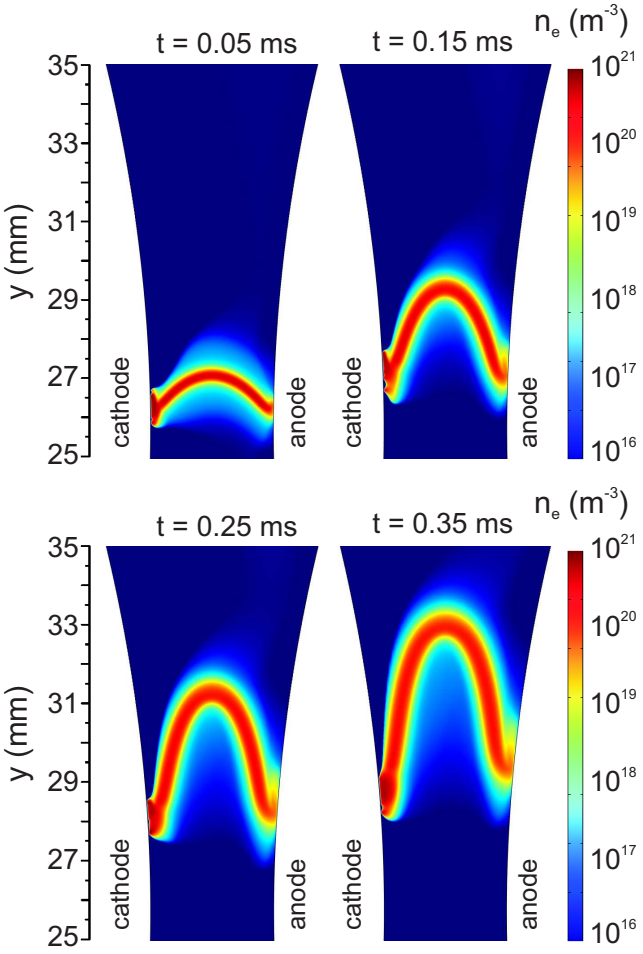

Figure 6. Electron density distribution, calculated with the 2D Cartesian model in the case of a glow discharge, at different moments in time, as noted in the figure. The following simulation parameters are used: FEF = 1, $\gamma_s = 0.02$, $R_b = 100\ \Omega$, $Us = 3700\ V$.

case of gas treatment for example. Indeed, the increased length leads to an increased plasma volume and thus to stronger plasma-gas interaction. In addition, the longer length means a higher voltage drop on the plasma channel which could cause earlier breakdown at the shortest distance between the electrodes. In this way, the attachment mechanism can also change the repetition rate of the discharge and this may also affect the gas treatment efficiency.

In spite of the differences in cathode "gliding" mechanisms and the resulting possible differences in the stretching of the arc, the overall plasma parameters and plasma channel characteristics still remain very similar in both regimes, determined primarily by the discharge current. Figure 8 shows the electron density along the y axis in the middle between cathode and anode. The density profiles coincide exactly at the early stage of the discharge development ($t = 0.05$ ms) and are only slightly displaced at the later stages ($t = 0.35$ ms) despite the fact that the cathode spot in the arc regime is completely immobile. Note that the same similarity is also observed (not shown here)

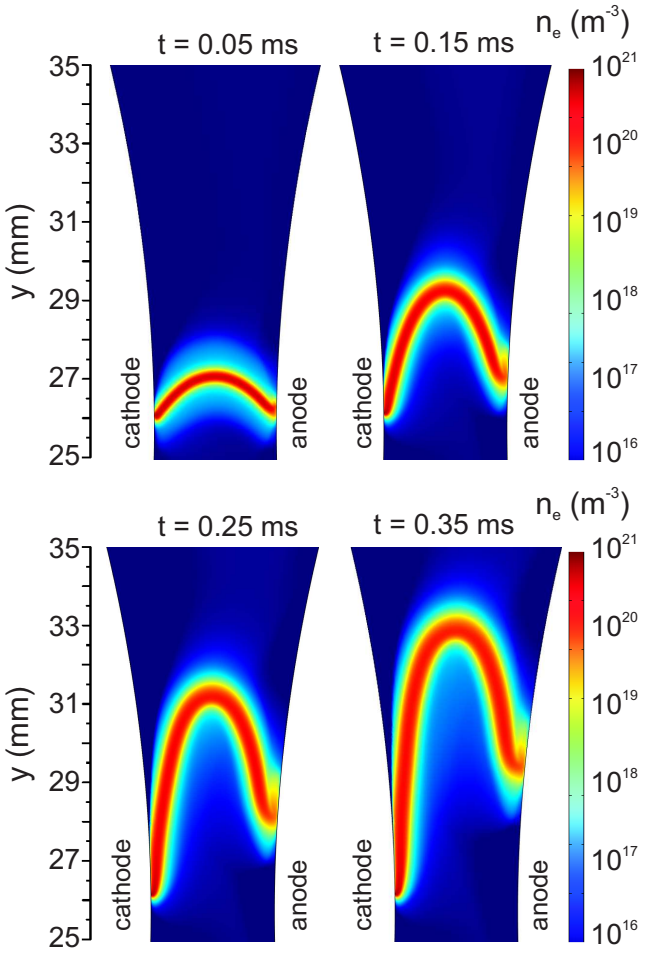

Figure 7. Electron density distribution, calculated with the 2D Cartesian model in the case of an arc discharge, at different moments in time, as noted in the figure. The following simulation parameters are used: FEF = 500, $\gamma_s = 0.02$, $R_b = 106.4\ \Omega$, $Us = 3700\ V$.

for the electron and gas temperatures, for the ion densities, etc.

4. Conclusions

The two different regimes of a gliding arc discharge, i.e., the arc and glow regime, are analyzed by means of 2D fluid models. The use of different models (Cartesian and axisymmetric) allows us to address different aspects of the discharge operation while preserving the computational time and the required resources to reasonable values. The obtained results show that the two regimes of discharge operation produce to a large extent a very similar plasma channel. Substantial differences are observed only in the proximity of the cathode. The differences are caused by the different electron emission mechanisms in both cases. The different properties of the plasma channel attachment to the cathode, however, can cause some differences between the two regimes. In the case of a glow discharge, the cathode root tends to follow the anode root. In the case of an arc

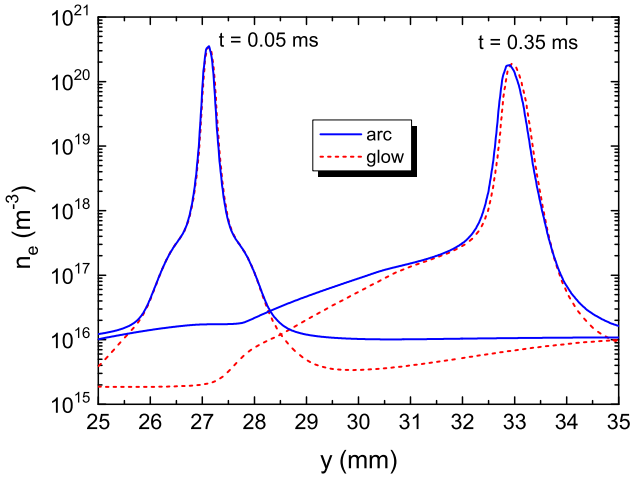

Figure 8. Electron density distribution along the y axis in the middle between cathode and anode, calculated with the 2D Cartesian model, at different moments in time, as noted in the figure.The simulation conditions are the same as in figure 6 for the glow discharge and figure 7 for the arc discharge.

operation, the cathode root usually remains connected to an electron emission center for a "long" period of time and it follows the anode root displacement in a stepwise manner, i.e. with jumps (new breakdowns). The distance between the consecutive spots (between successive "jumps") depends mainly on the surface properties of the cathode. If the cathode root is firmly attached to a certain emission center, the length of the plasma channel becomes much longer compared to the glow regime and this can have a different effect in gas treatment applications. Indeed, the longer length means an increased plasma volume and thus it leads to stronger plasma-gas interaction. Furthermore, also the discharge repetition rate may be affected by the cathode attachment mechanism, which might also affect the gas treatment efficiency.

In summary, the two discharge regimes tend to produce a plasma with similar properties, despite the fact that they consume rather different power. The arc regime seems to be more advantageous in terms of power efficiency due to the more efficient electron emission and the small cathode fall voltage. Moreover, it can produce a longer plasma channel, which can be desirable for certain applications, like gas treatment. However, the arc regime has a more erratic behavior and it is accompanied with sharp voltage drops during the cathode spot "jump", which might have a negative effect on the external circuit, like for example additional power losses in the power supply. The regime that will occur most in practice, and thus, the regime that should be considered in models as being most "realistic", will depend on the operating conditions and on the conditioning of the cathode.

5. Acknowledgements

This work is financially supported by the Methusalem financing and by the IAP/7 (Inter-university Attraction Pole) program "Physical Chemistry of Plasma-Surface Interactions" from the Belgian Federal Office for Science Policy (BELSPO). The work was carried out in part using the Turing HPC infrastructure of the CalcUA core facility of the Universiteit Antwerpen, a division of the Flemish Supercomputer Center VSC, funded by the Hercules Foundation, the Flemish Government (department EWI) and the Universiteit Antwerpen.

Appendix A. Model description

This appendix presents only the major governing equations of the models. Detailed description of the models can be found in the accompanying supporting information or in [5]. As noted in section 2, the models consider discharge in argon gas with argon kinetics similar to [5]. The governing equations of the Cartesian model are given below. The particle balance equations are within the drift-diffusion approximation:

$$\frac{\partial n_s}{\partial t} + \nabla \cdot \boldsymbol{G}_{\mathrm{s}} + (\boldsymbol{u}_{\mathrm{g}} \cdot \nabla) n_s = S_{\mathrm{c}}, \tag{A-1}$$

where n_s is the species density, $\boldsymbol{G}_{\mathrm{s}}$ is the species flux, $\boldsymbol{u}_{\mathrm{g}}$ is the gas velocity and S_c is the collision term representing the net number of particles produced or lost in the volume reactions. The index "s" represents all the species considered, except for the argon atoms, i.e. e, Ar^+, Ar_2^+, $\mathrm{Ar}\,(4\mathrm{s})$, $\mathrm{Ar}\,(4\mathrm{p})$, Ar_2^*. The argon gas atom density is considered to be constant.

The flux of the different species is expressed in the following way: the electron flux is $\boldsymbol{G}_{\mathrm{e}} = -D_e \nabla (n_e) + \frac{q_e}{|q_e|} \mu_e n_e \boldsymbol{E}$, the ion flux is $\boldsymbol{G}_{\mathrm{s}} = -D_s \nabla (n_s) + \frac{q_s}{|q_s|} \mu_s n_s \boldsymbol{E}$ and for the neutral species ($\mathrm{Ar}\,(4\mathrm{s})$,$\mathrm{Ar}\,(4\mathrm{p})$ and Ar_2^*) the flux is only determined by diffusion: $\boldsymbol{G}_{\mathrm{s}} = -D_s \nabla (n_s)$. In the above expressions, D is the diffusion coefficient and, μ is the mobility of the corresponding species, $\boldsymbol{E}$ is the electric field vector and q_s is the charge of the given species type.

The averaged electron energy $\overline{\varepsilon}_e$ is found by solving

$$\frac{\partial n_e \overline{\varepsilon}_e}{\partial t} + \nabla . \boldsymbol{G}_{\varepsilon,\mathrm{e}} + (\boldsymbol{u}_{\mathrm{g}} \cdot \nabla) n_e \overline{\varepsilon}_e = q_e \boldsymbol{E} . \boldsymbol{G}_{\mathrm{e}} + n_e \triangle \overline{\varepsilon}_e + Q_{\mathrm{bg}}, \tag{A-2}$$

where the electron energy flux is expressed as $\boldsymbol{G}_{\varepsilon,\mathrm{e}} = -D_{\varepsilon,e} \nabla (n_e \overline{\varepsilon}_e) - \mu_{\varepsilon,e} n_e \overline{\varepsilon}_e \boldsymbol{E}$. Here we use the following notations: $D_{\varepsilon,e}$ is the electron energy diffusion coefficient, $\mu_{\varepsilon,e}$ is the electron energy mobility and $\triangle \overline{\varepsilon}_e$ represents the averaged electron energy losses in the different collision events. $D_{\varepsilon,e}$ and $\mu_{\varepsilon,e}$ are derived from the electron mobility: $\mu_{\varepsilon,e} = (5/3)\mu_e$ and $D_{\varepsilon,e} = (2/3)\mu_{\varepsilon,e}\overline{\varepsilon}_e$. In order to improve the model numerical stability we add a constant background power density Q_{bg} everywhere in the simulated domain (i.e. the plasma and the neutral gas).

The electric field in the discharge is calculated with the Poisson equation:

$$\triangle \Phi = -\rho_{\mathrm{q}} / \varepsilon_0, \tag{A-3}$$

where Φ is the electric potential, $\rho_{\rm q}$ is the charge density and ε_0 is the vacuum dielectric permittivity.

An approximate solution for the gas flow velocity is obtained by solving the incompressible Navier-Stokes equations for a Newtonian fluid excluding the inertial term, i.e. in the regime of Stokes flow:

$$\rho_{\rm g}\frac{\partial \boldsymbol{u}_{\rm g}}{\partial t}=\nabla.(-p_{\rm g}\boldsymbol{I}+\mu_{\rm g}(\nabla \boldsymbol{u}_{\rm g}+(\nabla \boldsymbol{u}_{\rm g})^{\rm T})), \tag{A-4}$$

$$\rho_{\rm g}\nabla.\boldsymbol{u}_{\rm g}=0, \tag{A-5}$$

where $\rho_{\rm g}$ is the gas density, $p_{\rm g}$ is the gas pressure, $\mu_{\rm g}$ is the gas viscosity, $\boldsymbol{I}$ is the unit matrix and the superscript T stands for the tensor transpose operation.

The gas (heavy species) temperature is derived by solving the gas thermal balance

$$\rho_{\rm g}C_p\frac{\partial T_{\rm g}}{\partial t}+\rho_{\rm g}C_p\boldsymbol{u}_{\rm g}.\nabla T_{\rm g}-\nabla.\left(k_{\rm g}\nabla T_{\rm g}\right)=Q_{\rm g}, \tag{A-6}$$

where C_p is the gas heat capacity of Ar, $k_{\rm g}$ is the Ar thermal conductivity and $Q_{\rm g}$ is a heat source, which in our case results from the plasma heating. This includes all the energy lost by the electrons in elastic and inelastic collisions, which is assumed to be finally transferred to the gas, as well as the energy transferred from the ions to the gas. The ions gain energy from the electric field. The total gas heat source is thus expressed as:

$$Q_{\rm g}=\frac{3m_em_{Ar}}{\left(m_e+m_{Ar}\right)^2}n_en_{Ar}k_1e\left(T_e-T_{\rm g}\right)+\sum_i\triangle\varepsilon_ik_in_en_{i-t}+\boldsymbol{j}_{ion}\cdot\boldsymbol{E}, \tag{A-7}$$

where the first term represents the electron energy losses due to elastic collisions with rate coefficient k_1, the second term represents the sum of all electron energy losses due to inelastic collisions with energy loss $\triangle\varepsilon_i$, rate coefficient k_i and collision target density n_{i-t} for the i-th process, and the third term is the ion heating being the scalar product of the total ion current density $\boldsymbol{j}_{\rm ion}$ and the electric field $\boldsymbol{E}$.

The axisymmetric plasma model used here is based on equations (A-1), (A-2), (A-3) and (A-6), i.e. the same set of equations as the Cartesian model but excluding the gas flow description. As explained in section 2, the gas flow effect is replaced here by the addition of an effective loss terms in all balance equations (i.e. all except in the Poisson equation).

References

[1] Fridman A 2008, *Plasma Chemistry* (Cambridge: Cambridge University Press)

[2] Chernichowski A 1994 Gliding Arc. Applications to engineering and environment control *Pure and Appl. Chem.* **6** 1301-1310

[3] Nunnally T, Gutsol K, Rabinovich A, Fridman A, Gutsol A and Kemoun A 2011 *J. Phys. D: Appl. Phys.* **44**, 274009

[4] Korolev Y, Frants O, Landl N, Bolotov A and Nekhoroshev V 2014 Features of a near-cathode region in a gliding arc discharge in air flow. *Plasma Sources Sci. Technol.* **23** 054016

[5] Kolev St and Bogaerts A 2015 2D model for a gliding arc discharge *Plasma Sources Sci. Technol.* **24** 015025

[6] Tu X, Gallon H J and Whitehead J C 2011 Electrical and optical diagnostics of atmospheric pressure argon gliding arc plasma jet, 30th ICPIG, August 28th September 2nd 2011, Belfast, Northern Ireland, UK, C10

[7] Tu X, Gallon H J and Whitehead J C 2011 Dinamic behavior of atmospheric argon gliding arc plasma, *IEEE Trans. Plasma Sci.* **39** 2900-2901

[8] Latham R V and Xu N S Electron pin-holes: the limiting defect for insulating high voltages by vacuum, a basis for new cold cathode electron sources 1991 *Vacuum* **42** 1173-1181

[9] Richard F, Cormier J M, Pellerin S and Chapelle J 1997 Gliding arcs fluctuations and arc root displacement *High Temp. Mater. Processes* **1** 239-248

[10] Delair L, Brisset J L and Chéron B G Spectral electrical and dynamical analysis of a 50 Hz air gliding arc 2001 *High Temp. Mater. Processes* **5** 381-403.

Supporting information: Model description

St Kolev[1,2], A Bogaerts[1]

[1]Research group PLASMANT, Department of Chemistry, University of Antwerp, Universiteitsplein 1, B-2610 Antwerp, Belgium

[2]Faculty of Physics, Sofia University, 5 James Bourchier Boulevard, 1164 Sofia, Bulgaria

E-mail: skolev@phys.uni-sofia.bg

E-mail: annemie.bogaerts@uantwerpen.be

1. Argon kinetics

The argon kinetics taken into account in this work is similar to [1]. The model considers the following species: e – electrons, Ar – Argon atoms, Ar^+ – Argon ions, Ar_2^+ – Argon molecular ions, Ar (4s) – all 4s levels considered as a single lumped excitation level, Ar (4p) – all 4p levels considered as a single lumped excitation level, and Ar_2^* – which includes $Ar_2(^1\Sigma_u^+)$ and $Ar_2(^3\Sigma_u^+)$ excited molecules. The different processes considered in both models are listed in tables 1 and 2, along with the corresponding references for the rate coefficients and cross sections.

2. Cartesian model

The two models consider a slightly different set of equations, which is related to their specific aim and geometry. The 2D axisymmetric model considers the particle balance equations, the electron energy balance equation and the gas thermal balance. The 2D Cartesian model, on the other hand, considers the particle balance equations, the electron energy balance, the gas thermal balance and the Navier-Stokes equations for the gas flow description. In the following text we describe the equations used in the Cartesian model, as well as the boundary condition.

2.1. Particle balance equations

We use the drift-diffusion approximation and we solve the well-known particle balance equation:

$$\frac{\partial n_s}{\partial t} + \nabla \cdot \boldsymbol{G}_{\mathrm{s}} + (\boldsymbol{u}_{\mathrm{g}} \cdot \nabla) n_s = S_{\mathrm{c}}, \tag{1}$$

where n_s is the species density, $\boldsymbol{G}_{\mathrm{s}}$ is the species flux, $\boldsymbol{u}_{\mathrm{g}}$ is the gas velocity and S_c is the collision term representing the net number of particles produced or lost in the volume reactions included in tables 1 and 2. The index "s" represents all the species considered,

Table 1. Electron collisions included in the model.

Reaction	Rate coefficient	Reference
(R1) $e + Ar \rightarrow e + Ar$	BS[a]	[2]
(R2) $e + Ar \rightarrow e + Ar(4s)$	BS	[2]
(R3) $e + Ar \rightarrow e + Ar(4p)$	BS	[2]
(R4)[b] $e + Ar \rightarrow e + Ar(4d)$	BS	[2]
(R5) $e + Ar \rightarrow 2e + Ar^+$	BS	[2]
(R6) $e + Ar(4s) \rightarrow e + Ar(4p)$	BS	[3]
(R7) $e + Ar(4s) \rightarrow 2e + Ar^+$	BS	[4]
(R8) $e + Ar(4p) \rightarrow 2e + Ar^+$	BS	[4]
(R9) $e + Ar(4s) \rightarrow e + Ar$	BS, DB[c]	[2]
(R10) $e + Ar(4p) \rightarrow e + Ar$	BS, DB	[2]
(R11) $e + Ar(4p) \rightarrow e + Ar(4s)$	BS, DB	[3]
(R12) $Ar^+ + 2e \rightarrow Ar + e$	$k_{(m^6/s)} = 8.75 \times 10^{-39} T_e^{-4.5}(eV)$	[5]
(R13) $Ar^+ + e + Ar \rightarrow Ar + Ar$	$k_{(m^6/s)} = 1.5 \times 10^{-40} (T_g(K)/300)^{-2.5}$	[6]
(R14) $Ar_2^+ + e \rightarrow Ar^+ + Ar + e$	$k_{(m^3/s)} = 1.11 \times 10^{-12} \exp\left(-\frac{2.94-3(Tg(eV)-0.026)}{Te(eV)}\right)$	[7]
(R15) $Ar_2^+ + e \rightarrow Ar + Ar(4s)$	$k_{(m^3/s)} = 1.04 \times 10^{-12} [300/T_e(K)]^{0.67} \frac{1-\exp[-418/Tg(K)]}{1-0.31\exp[-418/Tg(K)]}$	[8,9]
(R16) $Ar_2^* + e \rightarrow Ar_2^+ + 2e$	$k_{(m^3/s)} = 9 \times 10^{-14} [T_e(eV)]^{0.7} \exp[-3.66/T_e(eV)]$	[10]
(R17) $Ar_2^* + e \rightarrow 2Ar + e$	$k_{(m^3/s)} = 1 \times 10^{-15}$	[10]

[a] Boltzmann solver: The rate coefficients are calculated from the corresponding cross sections, based on the solution of the Boltzmann equation with BOLSIG+ [11].

[b] This process is included only as an energy loss channel without considering the conservation equation for Ar(4d)

[c] Detailed balance: The rate coefficients for the superelastic processes are calculated using the detailed balance principle [12] incorporated in BOLSIG+ [11].

Table 2. Heavy species collisions and radiative transitions included in the model.

Reaction	Rate coefficient/collision frequency	Reference
(R18) $Ar(4s) + Ar(4s) \rightarrow Ar_2^+ + e$	$k_{(m^3/s)} = \frac{1}{2} 6.3 \times 10^{-16} (T_g(K)/300)^{-1/2}$	[13]
(R19) $Ar(4s) + Ar(4s) \rightarrow Ar^+ + Ar + e$	$k_{(m^3/s)} = 1.62 \times 10^{-16} (T_g(K))^{1/2}$	[14]
(R20) $Ar(4s) + Ar(4p) \rightarrow Ar^+ + Ar + e$	$k_{(m^3/s)} = 1.62 \times 10^{-16} (T_g(K))^{1/2}$	[14]
(R21) $Ar(4p) + Ar(4p) \rightarrow Ar^+ + Ar + e$	$k_{(m^3/s)} = 1.62 \times 10^{-16} (T_g(K))^{1/2}$	[14]
(R22) $Ar(4p) + Ar \rightarrow Ar(4s) + Ar$	$k_{(m^3/s)} = 5 \times 10^{-18}$	[15]
(R23) $Ar^+ + 2Ar \rightarrow Ar_2^+ + Ar$	$k_{(m^6/s)} = 2.5 \times 10^{-43} (T_g(K)/300)^{-3/2}$	[15]
(R24) $Ar_2^+ + Ar \rightarrow Ar^+ + 2Ar$	$k_{(m^3/s)} = \frac{6.06 \times 10^{-12}}{Tg(K)} \exp\left(-\frac{1.51 \times 10^4}{Tg(K)}\right)$	[7]
(R25) $Ar(4s) + 2Ar \rightarrow Ar_2^* + Ar$	$k_{(m^6/s)} = 3.3 \times 10^{-44}$	[10]
(R26) $Ar(4p) + 2Ar \rightarrow Ar_2^* + Ar$	$k_{(m^6/s)} = 2.5 \times 10^{-44}$	[15]
(R27) $Ar_2^* + Ar_2^* \rightarrow Ar_2^+ + 2Ar + e$	$k_{(m^3/s)} = 5 \times 10^{-16} (T_g(K)/300)^{1/2}$	[15]
(R28) $Ar_2^* + Ar(4s) \rightarrow Ar_2^+ + Ar + e$	$k_{(m^3/s)} = 6 \times 10^{-16} (T_g(K)/300)^{1/2}$	[15]
(R29) $Ar(4s) \rightarrow Ar + h\nu$	$\nu_{c(s^{-1})} = g_{eff}^a \times 3.145 \times 10^8$	[14]
(R30) $Ar(4p) \rightarrow Ar(4s) + h\nu$	$\nu_{c(s^{-1})} = 4.4 \times 10^7$	[14]
(R31) $Ar_2^* \rightarrow 2Ar + h\nu$	$\nu_{c(s^{-1})} = 6 \times 10^7$	[10]

[a] $g_{eff} = (1.15/\pi)\sqrt{(\lambda_{4s}/(6H))}$, where $\lambda_{4s} = 105.7$ nm and H is a characteristic dimension of the reactor, i.e., taken as $H = 3$ mm in our case.

except for the argon atoms, i.e. e, Ar^+, Ar_2^+, Ar (4s), Ar (4p), Ar_2^*. The argon gas atom density is considered to be constant.

The flux of the different species is expressed in the following way: the electron flux is

$$\boldsymbol{G}_{\rm e} = -D_e \nabla (n_e) + \frac{q_e}{|q_e|} \mu_e n_e \boldsymbol{E}, \tag{2}$$

the ion flux is

$$\boldsymbol{G}_{\rm s} = -D_s \nabla (n_s) + \frac{q_s}{|q_s|} \mu_s n_s \boldsymbol{E} \tag{3}$$

and for the neutral species (Ar (4s),Ar (4p) and Ar_2^*) the flux is only determined by diffusion: $\boldsymbol{G}_{\rm s} = -D_s \nabla (n_s)$. In the above expressions, D is the diffusion coefficient and, μ is the mobility of the corresponding species, $\boldsymbol{E}$ is the electric field vector and q_s is the charge of the given species type.

The transport coefficients used in the models are as follows: μ_e is derived from BOLSIG+ and the Ar^+ mobility is defined as in [16]:

$$\mu_{\rm Ar^+} = \frac{1.01 \times 10^5}{p_{\rm g}({\rm Pa})} \frac{T_g(K)}{273.16} 1.52 \times 10^{-4} \left({\rm m^2 V^{-1} s^{-1}} \right), \tag{4}$$

where $p_{\rm g}$ is the gas pressure and $T_{\rm g}$ is the gas temperature. The latter expression is also used for the molecular ion mobility with a certain correction factor [16], i.e. $\mu_{\rm Ar_2^+} = 1.2 \times \mu_{\rm Ar^+}$. The electron and ion diffusion coefficients are derived from their corresponding mobilities based on the Einstein relation. The Ar (4s) diffusion coefficient is defined according to [17] as

$$D_{\rm \ Ar(4s)} = (1/n_{\rm Ar}) 1.16 \times 10^{20} (T_{\rm \ Ar(4s)}(K)/300)^{1/2} \ \ ({\rm m^2/s}), \tag{5}$$

For the diffusion coefficients of Ar (4p) and Ar_2^*, due to the lack of literature data, we assume the same expression as for Ar (4s). This might look as a very rough approximation especially for Ar_2^*, but it does not significantly affect the final results because the diffusion terms in the balance equations for Ar (4p) and Ar_2^* remain negligible compared to the reaction terms. We also assume that the temperature of all heavy species is equal to the gas temperature ($T_{\rm g}$).

2.2. Averaged electron energy balance

The averaged electron energy is found by solving

$$\frac{\partial n_e \overline{\varepsilon}_e}{\partial t} + \nabla . \boldsymbol{G}_{\varepsilon,{\rm e}} + (\boldsymbol{u}_{\rm g} \cdot \nabla) n_e \overline{\varepsilon}_e = q_e \boldsymbol{E} . \boldsymbol{G}_{\rm e} + n_e \triangle \overline{\varepsilon}_e + Q_{\rm bg}, \tag{6}$$

where the electron energy flux is expressed as $\boldsymbol{G}_{\varepsilon,{\rm e}} = -D_{\varepsilon,e} \nabla (n_e \overline{\varepsilon}_e) - \mu_{\varepsilon,e} n_e \overline{\varepsilon}_e \boldsymbol{E}$. Here we use the following notations: $\overline{\varepsilon}_e$ is the electron averaged energy (averaged over the energy distribution function), $D_{\varepsilon,e}$ is the electron energy diffusion coefficient, $\mu_{\varepsilon,e}$ is the electron energy mobility and $\triangle \overline{\varepsilon}_e$ represents the averaged electron energy losses in the different collision events. $D_{\varepsilon,e}$ and $\mu_{\varepsilon,e}$ are derived from the electron mobility: $\mu_{\varepsilon,e} = (5/3)\mu_e$ and $D_{\varepsilon,e} = (2/3)\mu_{\varepsilon,e} \overline{\varepsilon}_e$. In order to make the numerical calculations more

stable, we add a constant background power density Q_{bg} everywhere in the simulated domain (i.e. the plasma and the neutral gas). In this way, in the whole domain we artificially sustain a low density plasma ($n_{\mathrm{e}} < 1 \times 10^{16}$ m^{-3}) with a certain temperature derived self-consistently (around 1.8 eV in the bulk). This power density is low enough so that it does not affect the arc behaviour, which is verified by several simulations with different background power Q_{bg}. The presence of background plasma allows us to significantly reduce the gradients in the variables between the arc and the background and thus to reduce the requirements to the discretization grid. The electron density due to this artificial heating is at least 4 orders of magnitude lower than the arc electron density.

2.3. Poisson equation

The electric field in the discharge is calculated with the Poisson equation:

$$\triangle\Phi = -\rho_{\mathrm{q}}/\varepsilon_0, \tag{7}$$

where Φ is the electric potential, ρ_{q} is the charge density and ε_0 is the vacuum dielectric permittivity.

2.4. Gas flow equations

For a proper description of the gliding arc we need to describe the gas flow which is responsible for the arc displacement. In the experiment considered here [18] the gas is supplied with a small nozzle positioned close to the shortest electrode distance position. With the 2D Cartesian model we are not able to accurately describe the gas flow from the nozzle. Therefore we solve here only a simplified version of the Navier-Stokes equations by adjusting the inlet boundary velocity in order to obtain a gas velocity similar to what is observed in the experiments. A rough estimation of the experimental gas velocity is obtained by examination of the arc displacement shown on successive high-speed photographs [18]. Note that this is, however, not a very accurate method since it is well possible that the arc does not have exactly the same velocity as the gas but slightly lower values [19, 20]. Note that measurements in [20] show that the gas-to-arc velocity ratio is in the order of 1.2-1.3. The equations solved are the incompressible Navier-Stokes equations for a Newtonian fluid excluding the inertial term, i.e. in the regime of Stokes flow:

$$\rho_{\mathrm{g}}\frac{\partial \boldsymbol{u}_{\mathrm{g}}}{\partial t} = \nabla.(-p_{\mathrm{g}}\boldsymbol{I} + \mu_{\mathrm{g}}(\nabla\boldsymbol{u}_{\mathrm{g}} + (\nabla\boldsymbol{u}_{\mathrm{g}})^{\mathrm{T}})), \tag{8}$$

$$\rho_{\mathrm{g}}\nabla.\boldsymbol{u}_{\mathrm{g}} = 0, \tag{9}$$

where ρ_{g} is the gas density, p_{g} is the gas pressure, μ_{g} is the gas viscosity, $\boldsymbol{I}$ is the unit matrix and the superscript T stands for the tensor transpose operation. In the model, the Navier-Stokes equations are not solved together with the other equations, because this would yield excessive calculations times, but instead they are solved first separately and then the obtained velocity distribution is used as input data.

2.5. Gas thermal balance

Here we calculate the gas temperature by solving the gas thermal balance

$$\rho_{\mathrm{g}} C_p \frac{\partial T_{\mathrm{g}}}{\partial t} + \rho_{\mathrm{g}} C_p \boldsymbol{u}_{\mathrm{g}} . \nabla T_{\mathrm{g}} - \nabla . \left(k_{\mathrm{g}} \nabla T_{\mathrm{g}} \right) = Q_{\mathrm{g}}, \tag{10}$$

where C_p is the gas heat capacity of Ar, k_{g} is the Ar thermal conductivity and Q_{g} is a heat source, which in our case results from the plasma heating. This includes all the energy lost by the electrons in elastic and inelastic collisions, which is assumed to be finally transferred to the gas, as well as the energy transferred from the ions to the gas. The ions gain energy from the electric field. The total gas heat source is thus expressed as:

$$Q_{\mathrm{g}} = \frac{3 m_e m_{Ar}}{\left(m_e + m_{Ar} \right)^2} n_e n_{Ar} k_1 e \left(T_e - T_{\mathrm{g}} \right) + \sum_i \triangle \varepsilon_i k_i n_e n_{i-t} + \boldsymbol{j}_{ion} \cdot \boldsymbol{E}, \tag{11}$$

where the first term represents the electron energy losses due to elastic collisions with rate coefficient k_1, the second term represents the sum of all electron energy losses due to inelastic collisions with energy loss $\triangle \varepsilon_i$, rate coefficient k_i and collision target density n_{i-t} for the i-th process, and the third term is the ion heating being the scalar product of the total ion current density $\boldsymbol{j}_{\mathrm{ion}}$ and the electric field $\boldsymbol{E}$. In the above expression the electron and gas temperatures are expressed in "eV". Here we neglect the energy loss due to radiation from excited atoms which is estimated to be relatively small (see also the comments in [5], page 277). The major term in equation (7) is usually the elastic energy transfer and only in the cathode layer the second and third terms in the right-hand side become considerable. The reason for the latter is the higher electron temperature in this region, enhancing the excitation processes, as well as the strong electric field which increases the ion velocity and the $(\boldsymbol{j}_{\mathrm{ion}} \cdot \boldsymbol{E})$ term.

In summary, the 2D Cartesian model includes equations (1), (6)-(10).

2.6. Boundary conditions

The boundary conditions (BC) are summarized in table 3 and some further explanation is given below.

The boundary condition for the electron balance equation (1) and the electron energy balance equation (6) at the cathode should include the electron emission processes in addition to the thermal flux. This yields the following BC for the normal electron flux at the cathode [21, 22]:

$$\boldsymbol{n} \cdot \boldsymbol{G}_{\mathrm{e}} = \frac{1}{2} \mathrm{v}_{\mathrm{e,th}} n_{\mathrm{e}} - \left[\sum_s \gamma_s \left(\boldsymbol{G}_s \cdot \boldsymbol{n} \right) + \boldsymbol{G}_{\mathrm{TF}} \cdot \boldsymbol{n} \right] \tag{12}$$

and for the normal electron energy flux [22]

$$\boldsymbol{n} \cdot \boldsymbol{G}_{\varepsilon,\mathrm{e}} = \frac{5}{6} \mathrm{v}_{\mathrm{e,th}} n_{\mathrm{e}} \overline{\varepsilon}_e - \left[\sum_s \gamma_s \varepsilon_{s,\mathrm{sec}} \left(\boldsymbol{G}_s \cdot \boldsymbol{n} \right) + \varepsilon_{\mathrm{TF}} \boldsymbol{G}_{\mathrm{TF}} \cdot \boldsymbol{n} \right] \tag{13}$$

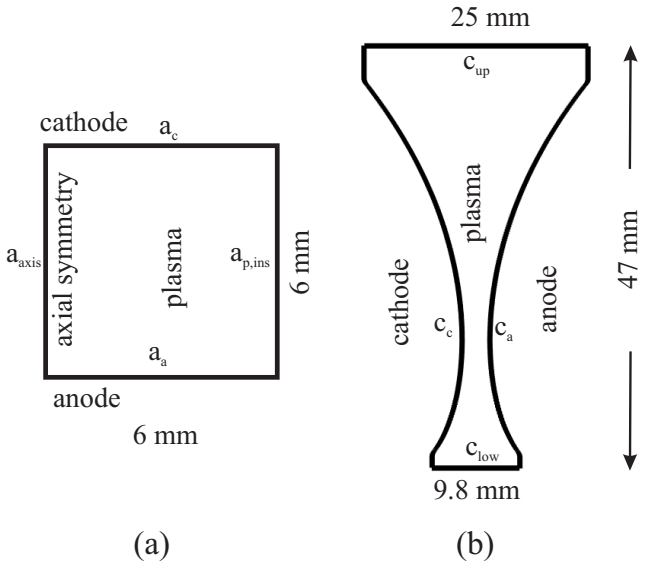

Figure 1. Geometries considered in the models:

(a) 2D axisymmetric model geometry with the following boundaries: a_c - cathode-plasma interface, a_a - anode, a_{axis} - axial symmetry axis, $a_{c,ins}$ - insulation boundary, $a_{p,ins}$ - insulation boundary for the plasma (zero fluxes).

(b) 2D Cartesian model geometry with the following boundaries: c_c - cathode, c_a - anode, c_{low} - upstream boundary used as a gas inlet, c_{up} - upper (downstream) boundary providing gas outflow.

In the above expressions $v_{e,th} = \sqrt{\frac{8k_BT_e}{\pi m_e}}$ is the electron thermal velocity, γ_s is the secondary electron emission coefficient due to ion impact for the two types of ions (Ar^+ and Ar_2^+) having a normal flux $\boldsymbol{G}_s$ towards the cathode. Hence, the sum is taken over these two types of ions. k_B is the Boltzmann constant, m_e is the electron mass, $\varepsilon_{s,sec}$ is the averaged energy of the secondary electrons and ε_{TF} is the averaged energy of the emitted electrons due to thermo-field emission. The value of γ_s is not known and it is very dependent on the cathode material and surface properties. $\boldsymbol{G}_{TF}$ is the electron flux due to thermo-field emission. It is known [23] that the combined effect of the thermal and field electron emissions (also denoted as thermo-field (TF) emission) is much stronger compared to the sum of both independent processes. Therefore, we use here the expression for the electron emission current density, which accounts for their combined effect [23]. It is also important to note that in the calculation of the field emission usually not the real normal electric field (E_n) is considered but an effective field which is calculated as $E_{n,eff} = \text{FEF} * E_n$. The factor FEF is called "Field enhancement factor" and accounts for the effective enhancement of the field due to surface roughness and sharp protrusions [23]. Similarly to γ_s, this factor will be very dependent on a particular experiment and it may even change during the experiments because of surface modification as a results of the arc impact.

For the non-emitting walls (anode and c_{up}) the BC includes only the thermal

electron flux:

$$\boldsymbol{n} \cdot \boldsymbol{G}_{\mathrm{e,n}} = \frac{1}{2} \mathrm{v}_{\mathrm{e,th}} n_{\mathrm{e}} \tag{14}$$

The electron energy flux in this case is then:

$$\boldsymbol{n} \cdot \boldsymbol{G}_{\varepsilon,\mathrm{e}} = \frac{5}{6} \mathrm{v}_{\mathrm{e,th}} n_{\mathrm{e}} \overline{\varepsilon}_e. \tag{15}$$

The ion flux at the walls, for both the Ar^+ and Ar_2^+ ions, is found by accounting for their thermal velocity and their drift velocity due to the electric field:

$$\boldsymbol{n} \cdot \boldsymbol{G}_s = \frac{1}{4} \mathrm{v}_{s,\mathrm{th}} n_s + \max\left(\frac{q_s}{|q_s|} \mu_s n_s \boldsymbol{E} \cdot \boldsymbol{n}, 0 \right) \tag{16}$$

where the function "max" returns the maximum of both arguments. In this case it sets the drift flux $\frac{q_s}{|q_s|} \mu_s n_s \boldsymbol{E} \cdot \boldsymbol{n}$ to 0 if it becomes negative, i.e. if the flux is directed towards the plasma domain. The neutral species, i.e. Ar(4s), Ar(4p) and Ar_2^*, are supposed to reach the wall due to thermal motion only and thus their BC on the wall is:

$$\boldsymbol{n} \cdot \boldsymbol{G}_s = \frac{1}{4} \mathrm{v}_{s,\mathrm{th}} n_s \tag{17}$$

where $s = \mathrm{Ar(4s)}, \mathrm{Ar(4p)}, \mathrm{Ar}_2^*$.

All these boundary conditions, as well as the other (more simple) boundary conditions, are summarised in tables 3 and 4.

Table 3. Boundary conditions used in the 2D Cartesian model, at the various boundaries (see figure 1); see text for the equation numbers. V_{c} is the cathode potential with respect to the grounded anode.

eq.	(1)	(1)	(1)	(6)	(7)	(8),(9)	(10)
variable	n_{e}	n_{Ar^+} $n_{\mathrm{Ar}_2^+}$	$n_{\mathrm{Ar(4s)}}$ $n_{\mathrm{Ar(4p)}}$ $n_{\mathrm{Ar}_2^+}$	$\overline{\varepsilon}_e$	Φ	$\boldsymbol{u}_{\mathrm{g}}$ p_{g}	T_{g}
c_c	(12)	(16)	(17)	(13)	$\Phi = V_{\mathrm{c}}$	$\boldsymbol{u}_{\mathrm{g}} = 0$	$T_{\mathrm{g}} = 293$ K
c_a	(14)	(16)	(17)	(15)	$\Phi = 0$	$\boldsymbol{u}_{\mathrm{g}} = 0$	$T_{\mathrm{g}} = 293$ K
$\mathrm{c}_{\mathrm{low}}$	$\boldsymbol{n} \cdot \alpha = 0$; $\alpha = \boldsymbol{G}_{\mathrm{s}}$, $\boldsymbol{G}_{\varepsilon,\mathrm{e}}$, $\nabla\Phi$					$\boldsymbol{n} \cdot \boldsymbol{u}_{\mathrm{g}} = 3$ m/s	$T_{\mathrm{g}} = 293$ K
c_{up}	(14)	$\boldsymbol{n} \cdot \nabla n_s = 0$		(15)	$\Phi = 0$	$p = 101$ kPa	$\boldsymbol{n} \cdot \nabla T_{\mathrm{g}} = 0$

Finally, we specify certain conditions for the external circuit and the power supply. In both models (Cartesian and Axisymmetric), the external circuit is represented by a fixed voltage source $V_{\mathrm{source}} = 3700$ V and serially connected resistor R_{b}.

3. Axisymmetric model

The axisymmetric plasma model used here is based on equations (1), (6), (7) and (10), i.e. the same set of equations as the Cartesian model, the gas flow which is excluded ($\boldsymbol{u}_\mathrm{g} = 0$). As explained in the manuscript, the gas flow effect is replaced here by the addition of an effective loss terms in all balance equations (i.e. all except in the Poisson equation). The aim of the additional loss terms is to effectively account for the stretching of the gliding discharge as a result of the gas flow and thus to account for the convective processes. The loss terms is introduced on the right hand side of equations 1, 6 and 10. These terms are introduced as effective loss processes with a constant frequency ν_elong, equal for all equations. Thus the loss terms will be proportional to $-\alpha\nu_\mathrm{elong}$, where α represents the conserved variable i.e. $\alpha = n_\mathrm{e}$, n_{Ar^+}, $n_{\mathrm{Ar}_2^+}$, $n_{\mathrm{Ar(4s)}}$, $n_{\mathrm{Ar(4p)}}$, $n_{\mathrm{Ar}_2^*}$, $n_\mathrm{e}\overline{\varepsilon}_\mathrm{e}$, $\rho_\mathrm{g}C_pT_\mathrm{g}$. ν_elong has a unit of frequency [1/s] but it is related to the elongation speed of the plasma channel. Below we give more details about the definition of ν_elong and its relation to the real convection process.

Let us consider an elementary domain with volume Ω and length l in the direction of elongation. As a result of the elongation with speed v_elong for time $\mathrm{d}t$, the plasma channel length will increase with $\mathrm{d}l = v_\mathrm{elong}\mathrm{d}t$ and the domain volume will increase with $\mathrm{d}\Omega = \mathrm{d}lS_\mathrm{tr}$, where S_tr is the transverse cross section of the plasma channel. If we take into account that for some variables there is a minimum (background) value (α_bg) different from zero (like for example the gas temperature $T_\mathrm{g} = 293$ K) we can express the variation (reduction) of the conserved variable α as the difference between the initial (α) and the value after elongation α_elong:

$$\mathrm{d}\alpha = \alpha_\mathrm{elong} - \alpha = \frac{\alpha\Omega + \alpha_\mathrm{bg}\mathrm{d}\Omega}{\Omega + \mathrm{d}\Omega} - \alpha = -\frac{(\alpha - \alpha_\mathrm{bg})\mathrm{d}\Omega}{\Omega + \mathrm{d}\Omega} \approx$$
$$-\frac{(\alpha - \alpha_\mathrm{bg})\mathrm{d}\Omega}{\Omega} = -(\alpha - \alpha_\mathrm{bg})\frac{\mathrm{d}l}{l} = -(\alpha - \alpha_\mathrm{bg})v_\mathrm{elong}\frac{\mathrm{d}t}{l} \tag{18}$$

Which is based on the fact that the variables are conserved i.e. $\alpha\Omega + \alpha_\mathrm{bg}\mathrm{d}\Omega = \alpha_\mathrm{elong}(\Omega + \mathrm{d}\Omega)$ and the fact that $\mathrm{d}\Omega \ll \Omega$. Thus for the effective loss term due to convection we obtain:

$$\frac{\mathrm{d}\alpha}{\mathrm{d}t} = -(\alpha - \alpha_\mathrm{bg})v_\mathrm{elong}/l = -(\alpha - \alpha_\mathrm{bg})\nu_\mathrm{elong} \tag{19}$$

The above approach allows us approximately to take into account the convection processes in the gliding discharge while representing the plasma channel by using a 2D axisymmetric model. In the model, we take α_bg to be zero for all variables except for the gas temperature: $T_\mathrm{g,bg} = 293$ K.

The geometry considered in this model is presented in figure 1(a). It is a simple rectangle with 6 mm distance between the electrodes.

References

[1] Kolev St and Bogaerts A 2015 2D model for a gliding arc discharge *Plasma Sources Sci. Technol.* **24** 015025

Table 4. Boundary conditions used in the 2D axisymmetric model, at the various boundaries (see figure 1); see text for the equation numbers.

eq.	(1)	(1)	(1)	(6)	(7)	(10)
variable	n_e	n_{Ar^+} $n_{\mathrm{Ar}_2^+}$	$n_{\mathrm{Ar(4s)}}$ $n_{\mathrm{Ar(4p)}}$ $n_{\mathrm{Ar}_2^+}$	$\overline{\varepsilon}_e$	Φ	T_g
$\mathrm{a_{p,ins}}$	$\boldsymbol{n}\cdot\alpha=0$; $\alpha=\boldsymbol{u}_\mathrm{g}$, $\boldsymbol{G}_\mathrm{s}$, $\boldsymbol{G}_{\varepsilon,\mathrm{e}}$, $\nabla\Phi$, ∇T_g					
a_c	(12)	(16)	(17)	(13)	$\Phi=V_c$	$T_\mathrm{g}=T_\mathrm{c}$
a_a	(14)	(16)	(17)	(15)	$\Phi=0$	$T_\mathrm{g}=293$ K
$\mathrm{a_{axis}}$	$\boldsymbol{n}\cdot\nabla\alpha=0$; $\alpha=n_\mathrm{s}$, $n_\mathrm{e}\overline{\varepsilon}_e$, Φ, T_g, T_c, Φ_cons					

[2] BIAGI-v7.1 database, www.lxcat.laplace.univ-tlse.fr; Transcribed from SF Biagi's Fortran code MAGBOLTZ, Version 7.1, 2004. http://consult.cern.ch/writeup/magboltz

[3] Bartschat K, Zeman V 1999 Electron-impact excitation from the (3p54s) metastable states of argon *Phys. Rev.* **A59** 2552

[4] Hyman H A 1979 Electron-impact ionization cross section for excited states of the rare gases (Ne, Ar, Kr, Xe), cadmium, and mercury *Phys. Rev. A* **20** 855-859

[5] Raizer Yu P, Gas Discharge Physics, (Berlin: Springer) p 62

[6] Dyatko N A, Ionikh Y Z, Kochetov I V, Marinov D L, Meshchanov A V, Napartovich A P, Petrov F B and Starostin S A 2008 Experiemntal and theoretical study of the transition between diffuse and contracted forms of the glow discharge in argon *J Phys* D: *Appl Phys* **41** 055204

[7] Jonkers J, van de Sande M, Sola A, Gamero A, Rodero A and van der Mullen J 2003 *Plasma Sources Sci. Technol.* **12** 464-474

[8] Cunningham A J, O'Malley T F and Hobson R M 1981 On the role of vibrational excitation in dissociative recombination *J. Phys.* B: *At. Mol. Phys.* **14** 773-782

[9] Castaños-Martinez E, Kabouzi Y, Makasheva K and Moisan M 2004 Modeling of microwave-sustained plasmas at atmospheric pressure with application to discharge contraction *Phys. Rev.* E **70** 066405

[10] Kannari F, Suda A, Obara M and Fujioka T 1983 Theoretical simulation of electron-beam-excited xenon-chloride (XeCl) Laser *IEEE J. Quant. Electron.* **19** 1587-1600

[11] Hagelaar G J M and Pitchford L C 2005 Solving the Boltzmann equation to obtain electron transport coefficients and the rate coefficients for fluid models *Plasma Sources Sci. Technol.* **14** 722-733

[12] Lieberman M A, Lichtenberg A J *Principles of Plasma Discharges and Materials Processing*, (Hoboken: John Wiley & Sons) 2005 p 267

[13] Bultel A, Ootegem B, Bourdon A and Vervisch P 2002 Influence of Ar_2^+ in argon collisional-radiative model *Phys. Rev.* E **65** 046406

[14] Gregório J, Leprince P, Boisse-Laporteand C and Alves L L 2012 Self-consistent modelling of atmospheric micro-plasmas produced by a microwave source *Plasma Sources Sci. Technol.* **21** 015013

[15] Lam S K, Zheng C-E, Lo D, Dem'yanov A and Napartovich A P 2000 Kinetics of Ar_2^* in high-pressure pure argon *J. Phys.* D: *Appl. Phys.* **33** 242-251

[16] Mcdaniel E W and Mason E A 1973 *The mobility and diffusion of ions in gases* (Wiley)

[17] Ferreira C M, Loureiro J and Ricard A 1985 Populations in the metastable and the resonance levels of the argon and stepwise ionization effects in a low-pressure argon positive column *J. Appl. Phys.* **57** 82-90

[18] Tu X, Gallon H J and Whitehead J C 2011 Electrical and optical diagnostics of atmospheric pressure argon gliding arc plasma jet, 30th ICPIG, August 28th September 2nd 2011, Belfast,

Northern Ireland, UK, C10

[19] Fridman A, Nester S, Kennedy L A Saveliev A and Mutaf-Yardemci O 1999 Gliding arc gas discharge *Progress in Energy and Combustion Science* **25** 211-231

[20] Richard F, Cormier J M, Pellerin S and Chapelle J 1996 Physical study of a gliding arc discharge *J. Appl. Phys.* **79** 22452250

[21] Hagelaar G J M, Fubiani G and Boeuf J-P 2011 Model of an inductively coupled negative ion source: I. General model description *Plasma Sources Sci. Technol.* **20** 015001

[22] Comsol Multiphysics 4.3a, Plasma module user's guide

[23] Jünter B, Puchkarev V F, Hantzsche E and Beilis I 1995 in *Hanbook of vacuum arc science and technology. Fundamentals and Applications* eds Boxman R, Sanders D M, Martin P M (Park Ridge, New Jersey: Noyes Publications) pp 158-174.